

# Fragmentation in Massive Star Formation

Henrik Beuther,<sup>1\*</sup> Peter Schilke,<sup>2</sup>

<sup>1</sup>Harvard-Smithsonian Center for Astrophysics, 60 Garden Street, Cambridge MA02138, USA

<sup>2</sup>Max-Planck-Institute for Astrophysics, Auf dem Huegel 69, 53121 Bonn, Germany

\*E-mail: hbeuther@cfa.harvard.edu.

**Studies of evolved massive stars indicate that they form in a clustered mode. During the earliest evolutionary stages, these regions are embedded within their natal cores. Here, we show high-spatial-resolution interferometric dust continuum observations disentangling the cluster-like structure of a young massive star-forming region. The derived protocluster mass distribution is consistent with the stellar initial mass function. Thus, fragmentation of the initial massive cores may determine the initial mass function and the masses of the final stars. This implies that stars of all masses can form via accretion processes, and coalescence of intermediate-mass protostars appears not to be necessary.**

There is a general consensus that massive stars ( $> 8 M_{\odot}$ ; solar masses) form exclusively in a clustered mode but the detailed physical processes are far from clear. While high enough accretion rates and accretion through disks are capable of forming massive stars, scenarios like the merging of intermediate-mass protostars at the dense centers of evolving clusters are also possible (1-3). Furthermore, one needs to understand why the stellar clusters have a universal mass spectrum fairly independent of environmental conditions, and how this mass spectrum evolves.

Therefore, it is crucial to study the earliest evolutionary stages at high spatial resolution, preferably in the mm-wavelength regime where dust emission is strong and optically thin, tracing all dust along the line of sight. The dust emission is directly proportional to the column density of dense gas within the regions, thus observing the mm continuum emission in very young massive star-forming regions allows us to study the gas and dust distributions, possible fragmentation of the larger scale cores, and physical parameters like masses and column densities.

Recently, we imaged dust continuum emission at 1.3 mm and 3 mm from the massive star-forming region IRAS 19410+2336 with the Plateau de Bure Interferometer [PdBI, (4)]. The region IRAS 19410+2336 is in an early stage of high-mass star formation prior to forming a hot core – a dense, hot clump of gas heated by a massive protostar (5). It is at a distance of  $\sim 2$  kiloparsec (kpc) and has an integrated bolometric luminosity of about  $10^4 L_{\odot}$  (solar luminosities). The region is part of a large sample of high-mass protostellar objects that has been studied extensively from cm to x-ray wavelengths (6-10).

The PdBI consists of six 15 m antennas, and we have observed the source in three different configurations with projected baseline lengths between 15 m and 330 m. The two-dimensional representation of projected baselines on the plane of the sky – the uv-plane – is covered extremely well in this range providing a high image fidelity at the corresponding spatial frequencies (11). At 1.3 mm the synthesized beam is  $1.5'' \times 1''$  and at 3 mm  $5.5'' \times 3.5''$ . Additionally, we present single-dish 1.2 mm observations of the same region obtained with the IRAM 30 m telescope at  $11''$  spatial resolution (7). Thus, we are able to analyze the evolving cluster at several spatial scales down to a linear resolution of 2000 astronomical units (AU,  $1''$  at a distance of 2 kpc).

The large scale emission observed at a wavelength of 1.2 mm with the IRAM 30 m telescope (Fig. 1a) shows two massive gas cores roughly aligned in a north-south direction. Based on the single-dish intensity profiles, we predicted that the cores should split up into sub-structures at

scales between  $3''$  and  $5''$  (7). PdBI 3 mm data at more than twice the spatial resolution show that both sources split up into sub-structures at the previously predicted scales, about four sources in the southern core and four in the northern core (Fig, 1b). At the highest spatial resolution (Figs. 1c and d), we observe that previously known gas clumps resolve into even more sub-sources. We find small clusters of gas and dust condensations with at least 12 sources per large scale core. Each of the protoclusters is dominated by one central massive source and surrounded by a cluster of less massive sources. This provides evidence for the fragmentation of a high-mass protocluster down to scales of 2000 AU at the earliest evolutionary stages.

In addition to a morphological interpretation, the data allow a quantitative analysis of the mass distribution. Assuming that the mm continuum is produced by optically thin thermal dust emission, one can calculate the masses and the column densities of the sub-sources following (12). The evolving protocluster is in a very early evolutionary state, and only the strongest source in the south exhibits weak (1 mJy) cm emission indicative of a recently ignited star (6,9). This cm emission is unresolved and does not affect the morphology of the dust emission. There could be temperature differences between various clumps as well as temperature gradients within individual clumps (13). However, in a massive cluster at the given distance it is difficult to obtain with current observational capabilities individual temperature estimates for each sub-source, let alone to derive internal clump temperature gradients. Nevertheless, due to the early evolutionary stage of the region prior to forming a significant hot core the dust temperatures throughout the cluster should not vary too strongly, and it is plausible to assume the same dust temperature for all sub-sources. Based on IRAS far-infrared observations, we estimate the average dust temperature to be around 46 K (6), the dust opacity index beta is set to 2 (7). The single-dish data (Figure 1a) reveal the overall gas mass, we derive  $840 M_{\odot}$  in the south and  $190 M_{\odot}$  in the north. Calculating the total masses for the southern and northern cluster from the interferometric data, we get lower values because the interferometers filter out the large scale

emission and trace only the most compact sources (11). This effect increases with decreasing wavelength. Thus, the 3 mm observations (Fig. 1b) still detect  $210 M_{\odot}$  in the south and  $80 M_{\odot}$  in the north, whereas at 1.3 mm we only observe the most compact condensations with a total mass of  $98 M_{\odot}$  in the south and  $42 M_{\odot}$  in the north (Figs. 1c and d). The data show that massive protocluster evolve in a core-halo fashion where the massive, dense gas clumps from which the stars are forming are embedded within a larger scale halo of more broadly distributed gas. A fraction of 80-90% of the total gas mass appears to be associated mostly with the halo.

More interesting than the total core masses are the individual masses and column densities of each sub-source. In the 1.3 mm PdBI data we identify 12 individual clumps above the  $3\sigma$  level of 9 mJy/beam in each of the southern and northern cores. At the assumed temperature of 46 K, the  $3\sigma$  level corresponds to a clump-mass sensitivity of  $\sim 1.7 M_{\odot}$ , and the derived clump masses range between  $1.7 M_{\odot}$  and  $25 M_{\odot}$ . The calculated peak column densities are of the order  $10^{24} \text{cm}^{-2}$  corresponding to a visual extinction  $A_v$  of about 1000. Such an extinction is too high to be penetrated by near-infrared, mid-infrared or even hard x-ray emission. Our sample is sensitivity limited for individual gas clumps below  $1.7 M_{\odot}$ . We do not believe that the spatial filtering property of the interferometric observing technique affects our results, because the scales of all, even the most massive clumps (of order a few arcsec) is far smaller than the spatial structures filtered out (of sizes above 20 arcsec). Consequently, only a large-scale halo common to all sources is affected by the filtering, while the sources we are interested in are not.

Combining the data from both clusters, we derive a mass spectrum of the protocluster (Figure 2). The best fit to the data results in a mass spectrum  $\Delta N/\Delta M \sim M^{-a}$  with a power-law index  $a = 2.5$  and a mean deviation  $da = 0.3$ . A potential uncertainty for the slope of the spectrum is the assumption of uniform dust temperatures for all sub-sources: while higher temperatures for the more massive clumps would decrease these derived masses, lower temperatures

for the less massive clumps would increase those mass estimates. These effects would result in a somewhat flattened slope. However, as argued before, we infer from the early evolutionary state of IRAS 19410+2336 that the dust temperature distribution should not vary strongly, and we conclude that the relative accuracy between the derived clump masses – and thus the slope of the mass spectrum – is high. This derived power-law index  $a$  can directly be compared with the initial mass function (IMF) results obtained for more evolved clusters. While there has been a lot of discussion about the very low-mass end ( $< 1 M_{\odot}$ ) there is a general consensus that the IMF for stars  $> 1 M_{\odot}$  can be approximated by  $a = 2.5 \pm 0.2$  (1,14-17). Furthermore, in a study of low-mass protostars in  $\rho$  Ophiuchus, it was found that the mass spectrum of protostars between  $0.5 M_{\odot}$  and  $3 M_{\odot}$  can be approximated by  $a = 2.5$  (18). While the observations of  $\rho$  Ophiuchus already suggested that the IMF of low-mass stars is determined at early evolutionary stages, this was far from clear for massive clusters because merging of intermediate-mass protostars could form the IMF at later stages as well (2). Our new data now indicate that the IMF of high-mass clusters is also determined at the earliest stages of evolution. An IMF determined at the very beginning of the cluster formation is support for the disk-accretion scenario for stars of all masses, because coalescence would probably occur at later stages and could hardly know anything about the initial fragmentation processes. However, these data do not rule out the possibility that coalescence of intermediate-mass protostars might occur within the dense centers of individual sub-cores.

## References and Notes

1. R.E. Pudritz, Science 295, 68 (2002).
2. S.W. Stahler, F. Palla, P.T.P. Ho. Protostars and Planets IV pp.327-+ (2000).
3. C.F. McKee, J.C. Tan. Nature 416. 59 (2002).
4. S. Guilloteau, et al., A&A 262, 624 (1992).
5. S. Kurtz, R. Cesaroni, E. Churchwell, P. Hofner, C.M. Walmsley, Protostars and Planets IV

pp. 299-+ (2000).

6. T.K. Sridharan, H. Beuther, P. Schilke, K.M. Menten, F. Wyrowski, *ApJ* 566, 931 (2002).

7. H. Beuther, et al., *ApJ* 566, 945 (2002).

8. H. Beuther, et al., *A&A* 383, 892 (2002).

9. H. Beuther, J. Kerp, T. Preibisch, T. Stanke, P. Schilke, *A&A* 395, 169 (2002).

10. H. Beuther, P. Schilke, T. Stanke, *A&A* 408, 601 (2003).

11. G.B. Taylor, C.L. Carilli, R.A. Perley, eds., *Synthesis Imaging in Radio Astronomy II* (1999).

12. R.H. Hildebrand, *QJRAS* 24, 267 (1983).

13. F.C. Adams, F.H. Shu, *ApJ* 296, 655 (1985).

14. E.E. Salpeter, *ApJ* 121, 161 (1955).

15. G.E. Miller, J.M. Scalo, *ApJS* 41, 513 (1979).

16. J. Scalo, *ASP Conf. Ser. 142: The Stellar Initial Mass Function (38th Herstmonceux Conference)* (1998), pp. 201-+.

17. P. Kroupa, C.A. Tout, Gilmore G., *MNRAS* 262, 545 (1993).

18. F. Motte, P. Andre, R. Neri, *A&A* 336, 150 (1998)

19. Based on observations with the IRAM Plateau de Bure Interferometer and the 30 m. IRAM is supported by INSU/CNRS (France), MPG (Germany), and IGN (Spain). We thank an unknown referee for very helpful comments improving the paper. H.B. acknowledges financial support by the Emmy-Noether-Programm of the Deutsche Forschungsgemeinschaft (DFG, grant BE2578/1).

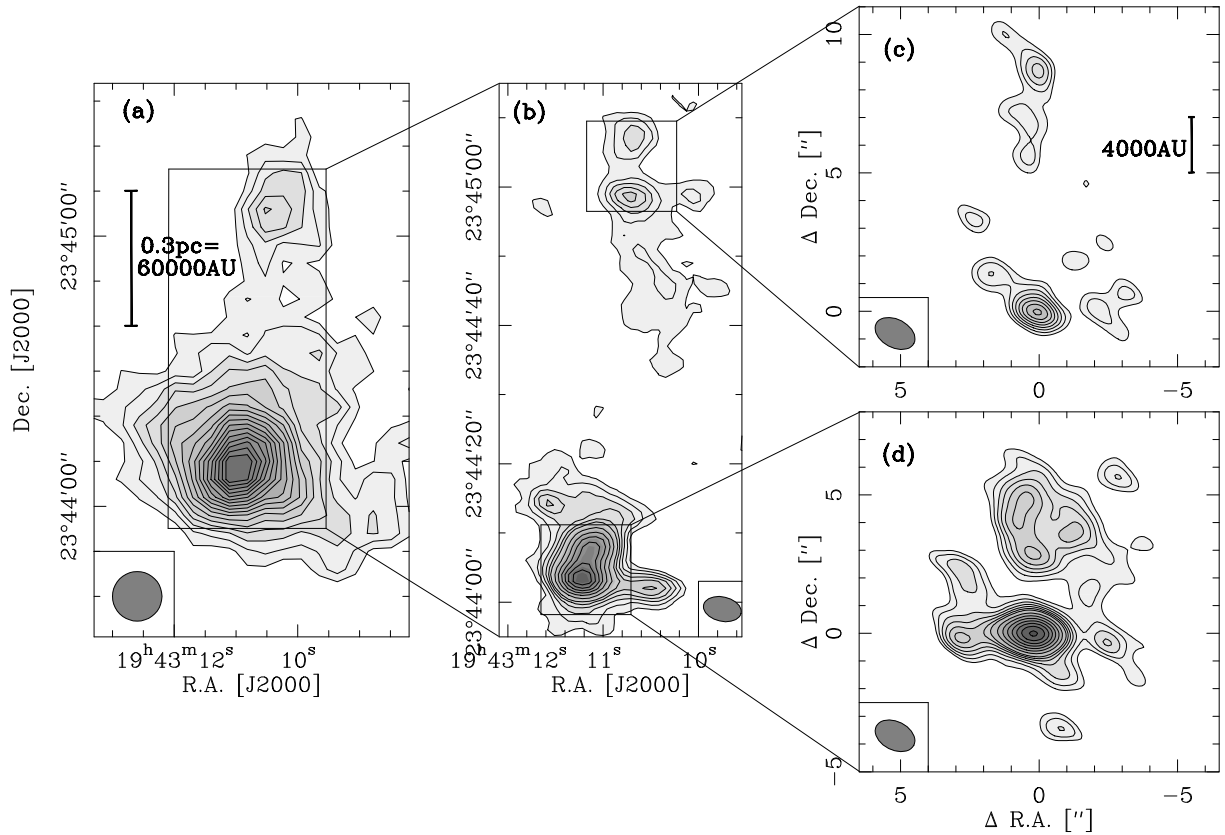


Fig. 1: Dust continuum images of IRAS 19410+2336. The left image shows 1.2 mm single-dish data obtained with the IRAM 30 m at low spatial resolution (7). The middle and right images present the 3 mm and 1.3 mm PdBI data obtained with a spatial resolution nearly an order of magnitude better. The beams are shown at the bottom left or right of each panel, respectively. The contouring of (a) starts at 15% of the peak flux increasing in 5% intervals, (b) is contoured in 5% intervals of the peak flux between 5% and 25%, and in 10% intervals between 30% and 90%. The 1.3 mm images in Figures (c) and (d) are contoured at  $1\sigma$  steps between the  $3\sigma$  level of 9 mJy and 27 mJy, and at  $2\sigma$  steps above that.

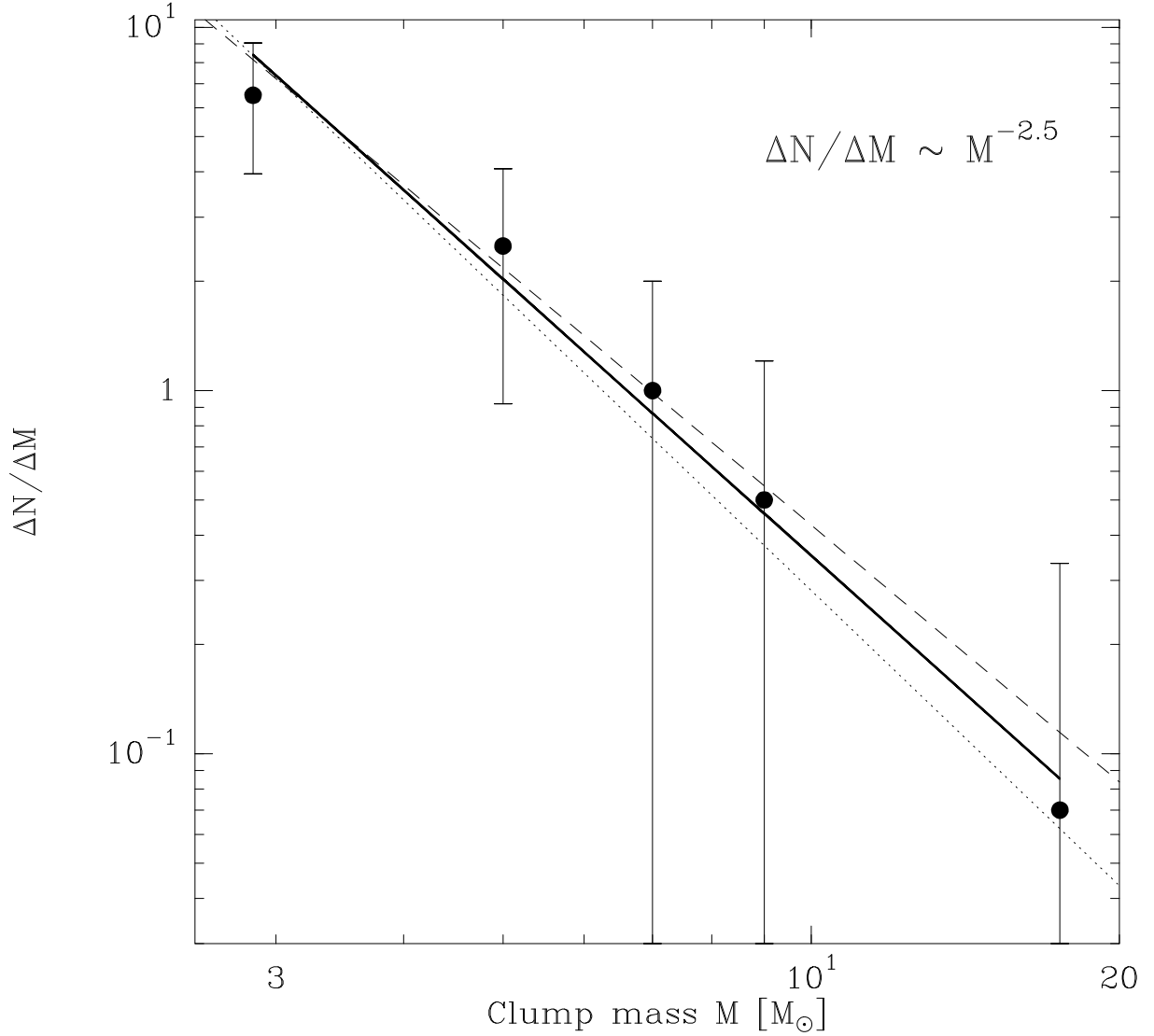


Fig. 2: The mass spectrum of IRAS 19410+2336. The clump-mass bins are  $[1.7(3\sigma), 4]$ ,  $[4, 6]$ ,  $[6, 8]$ ,  $[8, 10]$  and  $[10, 25]$   $M_{\odot}$ , the axes are in logarithmic units. The error-bars represent the standard deviation of a Poisson-distribution  $\sqrt{\Delta N / \Delta M}$ . The solid line shows the best fit to the data  $\Delta N / \Delta M \sim M^{-a}$  with  $a = 2.5$ . The dashed and dotted lines present the IMFs derived from Salpeter with  $a = 2.35$  (14) and Scalo with  $a = 2.7$  (16), respectively.